https://doi.org/10.5194/essd-2026-52
Preprint. Discussion started: 20 March 2026

Open Access Earth System Science Data Discussions

Global dynamic precipitation isoscapes over three-quarters of a century

Ikuya Adachi[1], Tsutomu Yamanaka[2]

[1]Degree Programs in Life and Earth Sciences, University of Tsukuba, 1-1-1 Tennodai, Tsukuba, Ibaraki 305-8572, Japan
[2]Institute of Life and Environmental Sciences, University of Tsukuba, 1-1-1 Tennodai, Tsukuba, Ibaraki 305-8572, Japan

Correspondence to: Ikuya Adachi (adachi.ikuya.ss@alumni.tsukuba.ac.jp)

Abstract.

Stable precipitation isotopes are widely used as tracers in water cycling and material transport. However, observational networks (e.g., the Global Network of Isotopes in Precipitation, or GNIP) are sparse in space and time, constraining analyses and applications in data-poor regions. To bridge this gap, static isoscapes, which interpolate monthly observations to long-term annual or climatological monthly means, have been developed and applied across disciplines. In recent years, growing interest in event-scale processes and isotope-enabled hydrological modeling has increased the need for higher-frequency information.

In this study, a global precipitation isoscape using an offline isotope circulation model (ICM) forced by JRA-3Q on a 1.25° grid covering −80° to 80° of latitude is produced. The deliverables include daily values, precipitation-weighted monthly values, and climatological monthly means for 1948–2023; the daily and monthly time series cover September 1947 to March 2024. GNIP-based validation demonstrates high skill for climatology. When all the station–month pairs are analyzed in a single regression, R^2 equals 0.86 for $\delta^{18}O$ and 0.87 for $\delta^{2}H$, with root-mean-square errors (RMSEs) of 2.02‰ and 16.0‰, respectively. At the monthly scale, unweighted averaging of station-level metrics yields R^2 values of 0.47 and 0.48, with RMSEs of 2.62‰ and 19.9‰, respectively. Daily performance was quantified from same-day regional means in East Asia and from 21 GNIP stations not used in the correction; R^2 is typically between 0.3 and 0.6, and the RMSE is between 2 and 4‰ for $\delta^{18}O$. By comparison, d-excess exhibits lower global skill, likely reflecting sensitivity to uncertainties in the forcing and to model simplifications.

In contrast to observation-interpolated static isoscapes, this reanalysis-driven dataset delivers seamless coverage, including data-sparse regions, with explicitly characterized error properties. The data are distributed as NetCDF/CSV (daily, monthly) and GeoTIFF (climatology) and support applications from isotope-enabled hydrology and source attribution to climate-impact assessments and global water-resource analyses.

1 Introduction

Stable precipitation isotopes are widely used to trace terrestrial water cycling and the transport of materials (Kendall and Caldwell, 1998; Bowen et al., 2005). Most measurements have been made at monthly resolution, as in the Global Network of

https://doi.org/10.5194/essd-2026-52
Preprint. Discussion started: 20 March 2026

Isotopes in Precipitation (GNIP). However, the station network is spatially sparse, which constrains tracer studies in regions lacking observations. To mitigate this limitation, statistical, geostatistical, or hybrid isoscape models have been developed that interpolate monthly observations (e.g., Bowen and Wilkinson, 2002; Bowen, 2010; Vachon et al., 2010; Terzer-Wassmuth et al., 2021). These products depict global-to-regional fields as long-term annual or climatological monthly means and are therefore commonly regarded as static isoscapes. Related machine-learning approaches have likewise been used to reconstruct multidecadal monthly fields (Nelson et al., 2021). Their usefulness has been demonstrated across disciplines, from hydrology to ecology and forensic applications (e.g., Hobson et al., 2010; Ehleringer et al., 2010; Adachi and Yamanaka, 2024).

In parallel, the demand for higher-frequency information has increased as studies increasingly target event-scale hydrological processes (Birkel et al., 2012; Stevenson et al., 2021). In response, Adachi and Yamanaka (2025a) refined the isotope circulation model (ICM; developed by Yoshimura et al., 2003) and evaluated its ability to reproduce day-to-day variability across three mid-latitude East Asian regions during June–September, the hydrologically active period defined by the monsoon rainy-season climatology (Wang and LinHo, 2002). Unlike isotope-enabled general circulation models (isoGCMs; Joussaume et al., 1984; Sturm et al., 2010), which cannot capture the stochastic nature of weather without dynamical nudging (Yoshimura et al., 2008), the offline ICM is driven by atmospheric reanalyses and explicitly computes water and isotope budgets. Because atmospheric reanalyses assimilate observations, they better represent actual meteorology at short time scales, making the offline ICM well suited for simulating daily or event-scale isotope variability. With explicit land-surface isotope processes and postcondensational effects (e.g., subcloud raindrop evaporation), the refined ICM successfully reproduced daily isotope variations in East Asia, especially in maritime climates such as the Kanto Plain.

Here, we extend the validation of the refined ICM to the global domain and generate a multidecadal dataset of precipitation isotopes that includes daily values, precipitation-weighted monthly values, and climatological monthly means. The dataset is distributed in NetCDF and CSV formats to facilitate both spatial analyses and pointwise time series applications. The resulting dataset ($\delta^{18}O$, $\delta^{2}H$, and d-excess) is designed to support a wide range of isotope-enabled studies from regional to global scales and across timescales from day-to-day variability to seasonal changes.

2 Methods

2.1 Model simulations

We generated dynamic precipitation isoscapes using the isotope circulation model (ICM) developed and evaluated by Adachi and Yamanaka (2025). A schematic overview of the model is shown in Figure 1, while the full model description is provided in Supplementary Methods S1.

The ICM is based on the framework originally proposed by Yoshimura et al. (2003) and incorporates isotopic variability associated with surface evaporation and subcloud raindrop evaporation. Meteorological forcing was taken from the JRA-3Q reanalysis dataset (Kosaka et al., 2024).

https://doi.org/10.5194/essd-2026-52
Preprint. Discussion started: 20 March 2026

Open Access Earth System Science Data Discussions

Simulations were conducted continuously for 76 years, from September 1947 to March 2024, with an hourly time step. Daily precipitation isotope outputs were aggregated into precipitation-weighted monthly means, climatological monthly means, and annual means.

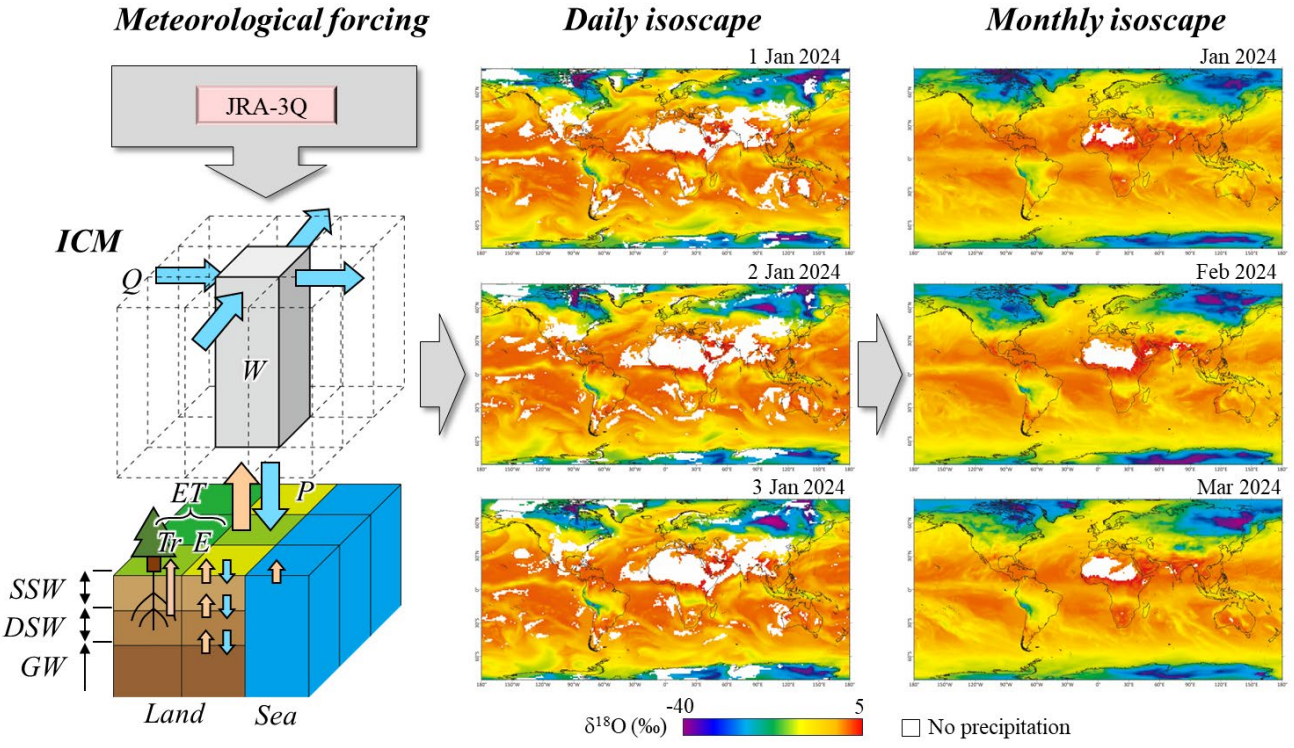

Figure 1: Schematic of the isotope circulation model

https://doi.org/10.5194/essd-2026-52
Preprint. Discussion started: 20 March 2026

Open Access Earth System Science Data Discussions

2.2 Corrections

To improve the usability of the ICM outputs as a precipitation isoscape dataset, we identified and corrected spatially systematic biases. The bias-correction procedure is designed to reduce large-scale systematic offsets while preserving the temporal variability produced by the dynamical model. Using GNIP observations as the reference, we calculated the difference between the observed GNIP values and the ICM output and used that difference as the correction term. GNIP stations were included if they provided at least two isotope–precipitation pairs per month to avoid corrections dominated by singular events and to estimate representative mean corrections. The GNIP stations used for corrections are shown in Fig. 2. In total, 481 stations for $\delta^{18}O$, 441 for $\delta^{2}H$, and 435 for d-excess met the criterion.

We computed monthly bias values for January through December at each station and then took their arithmetic mean to obtain an annual-mean correction. Because GNIP stations are spatially sparse, we generated a global correction map via inverse-distance-weighting (IDW) interpolation in ArcGIS. We then applied this map to the ICM outputs (daily, monthly, and climatological) to obtain annually bias-corrected precipitation isoscapes. For clarity of sign, bias was defined as ICM − GNIP, and the correction consisted of subtracting this bias field from the ICM output.

Bias correction was performed independently for $\delta^{18}O$, $\delta^{2}H$, and d-excess. Although d-excess can be derived from $\delta^{18}O$ and $\delta^{2}H$, a previous study revealed that the reproducibility of d-excess is insufficient (Adachi and Yamanaka, 2025a). Therefore, simply correcting $\delta^{18}O$ and $\delta^{2}H$ and then recomputing d-excess would not be expected to meaningfully improve performance; thus, we independently corrected d-excess. The global correction map is shown in Fig. 3.

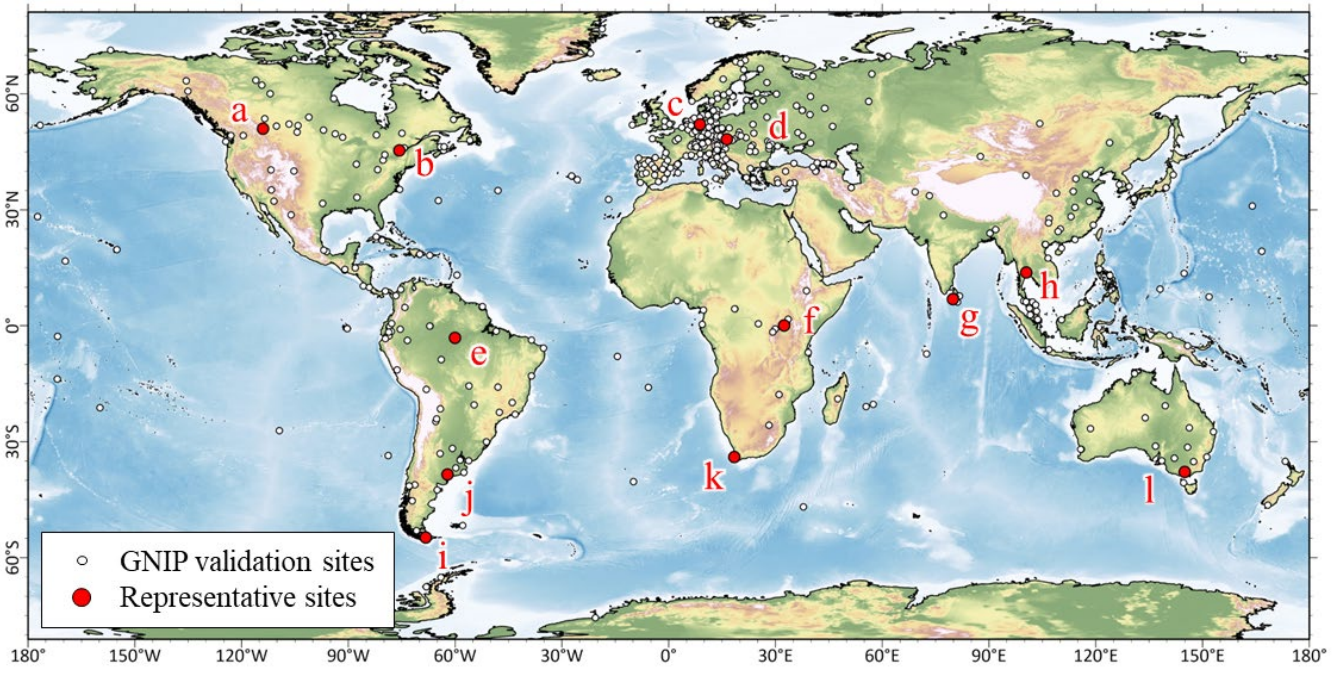

Figure 2: GNIP stations used for bias correction and validation (open circles). Red dots mark representative sites illustrated in Figs. 8 and 10.

https://doi.org/10.5194/essd-2026-52
Preprint. Discussion started: 20 March 2026

Open Access Earth System Science Data Discussions

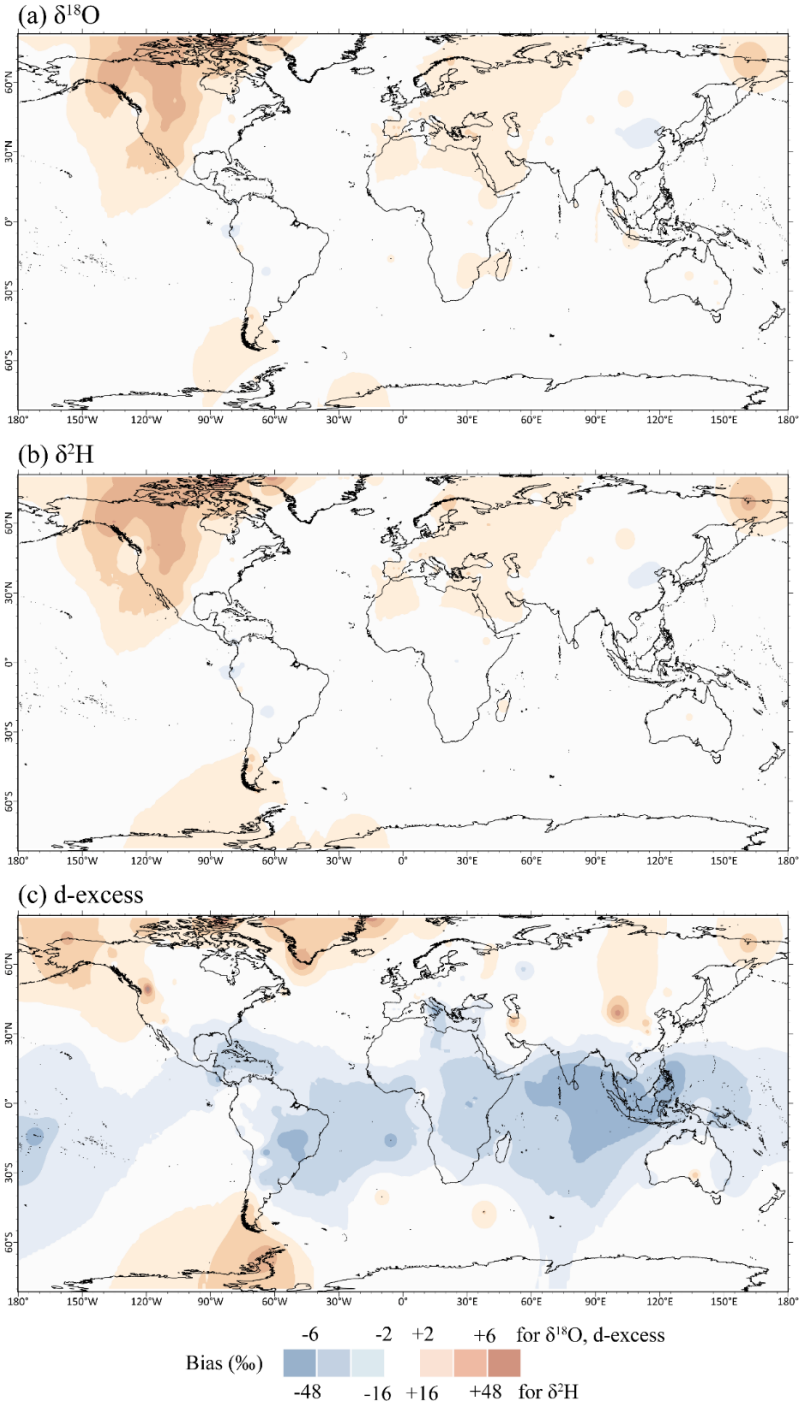

Figure 3: Spatial distribution of the annual mean bias: (a) $\delta^{18}O$, (b) $\delta^{2}H$, and (c) d-excess. These bias values are used as correction offsets. Positive bias indicates ICM > GNIP.

https://doi.org/10.5194/essd-2026-52
Preprint. Discussion started: 20 March 2026

2.3 Validations

We validated the dataset against GNIP observations. For climatological and monthly scales, we compared observations with the collocated model grid-cell values using the same station set as in the bias correction. To prevent information leakage that would inflate skill estimates, we adopted a leave-one-out jackknife: for each target station, we recomputed the annual-mean correction without that station before evaluating errors at its location. We quantified skill using the coefficient of determination (R^2) and the root-mean-square error (RMSE) relative to the observations. We then interpolated the stationwise R^2 and RMSE fields using inverse distance weighting (IDW) to produce global skill maps. To benchmark the ICM against other dynamical isoscape models, we also compared our results with nudged isotope-enabled GCM outputs from SWING2 (Risi et al., 2012). For an observation-based baseline, we further evaluated it against a widely used static global isoscape constructed from GNIP observations (Bowen et al., 2005). In addition, we selected 12 GNIP stations with relatively long records from three latitude bands and treated them as representative sites (Fig. 2). The bands include Northern Hemisphere mid- to high latitudes, low latitudes, and Southern Hemisphere mid- to high latitudes.

Daily skill in East Asia was evaluated following Adachi and Yamanaka (2025a). That study assessed the uncorrected ICM; here, we reevaluate it using bias-corrected fields and report the precorrection results for comparison. Within each region (Kanto Plain, North China Plain, Mongolian Plateau; Yamanaka et al., 2001, 2004, 2007), we calculated same-day/event regional means by averaging precipitation-isotope observations from multiple sites and compared these with regional means from the model on matching dates. This averaging suppresses subgrid-scale variability, making the protocol suitable for daily scale assessment. Because publicly available concurrent multisite daily datasets do not exist in GNIP, a global application of the above protocol was not feasible. Instead, for GNIP stations that provide daily observations, we computed stationwise daily skill as a reference: stations with at least 100 daily samples were retained; model–observation pairs were formed on matching dates at the colocated grid cell; and R^2 and RMSE were calculated. We selected 21 stations that were not used in the bias correction for this evaluation. These stationwise metrics can be influenced by subgrid variability and should therefore be interpreted with appropriate caution.

https://doi.org/10.5194/essd-2026-52
Preprint. Discussion started: 20 March 2026

3 Data records

We provide a global dataset of precipitation isotopic compositions computed with ICM and postprocessed using an annual-mean bias correction derived from GNIP stations. The spatial domain covers the globe except for high latitudes poleward of 80° in both hemispheres on a 1.25° × 1.25° longitude–latitude grid (WGS 84; longitudes −180° to 180°). Three temporal products are delivered: (i) climatological monthly means of $\delta^{18}O$, $\delta^{2}H$, and d-excess defined as arithmetic means for January 1948–December 2023; (ii) precipitation-weighted monthly values; and (iii) daily values. The daily and monthly series span September 1947–March 2024.

Files are distributed in three formats. Daily and monthly values are provided in NetCDF and CSV. The monthly NetCDF files package the full period and global domain into a single file, whereas the daily NetCDF files are organized as one file per calendar month. For pointwise analyses, CSV files are organized as one file per grid cell and contain time series of $\delta^{18}O$, $\delta^{2}H$, and d-excess for the entire period. CSV files follow a consistent latitude/longitude-based naming scheme to support reproducibility. Climatological monthly means are also supplied as GeoTIFFs to facilitate GIS workflows.

The climatological $\delta^{18}O$ pattern (Fig. 4) shows enrichment at low latitudes and depletion toward high latitudes (latitude effect), stronger depletion over continental interiors (inland effect), a clear seasonal imprint in the Northern Hemisphere (temperature effect), an amount effect in tropical convective regions, and altitude-related depletions along major orographic systems (e.g., Himalaya–Tibet, Andes, and the European Alps), which are consistent with established isotope–climate relationships.

At 35°N, 140°E (Tokyo region), a representative time series exhibits a climatological annual cycle (Fig. 5a–c) with relatively enriched winter values and depleted values during the June–July rainy season and the September–October typhoon season. The d-excess cycle peaks in winter and weakens in summer. The multiyear monthly series (Fig. 5d–f) follow the same phase with notable interannual spread; in the Kanto region, the typical standard deviations are ~1.5‰ for $\delta^{18}O$ and ~10‰ for $\delta^{2}H$. The daily series (one illustrative year; Fig. 5g–i) reveals event-scale variability of approximately 0 to −10‰ in $\delta^{18}O$ and +10 to −80‰ in $\delta^{2}H$. Because the dataset is driven by meteorological reanalysis and constrained by station-based bias correction, it provides time-varying isotope information in data-sparse regions while remaining consistent with observed climatological means and seasonal variability. Users should consider grid-cell representativeness, particularly for daily values that are sensitive to subgrid processes.

https://doi.org/10.5194/essd-2026-52
Preprint. Discussion started: 20 March 2026

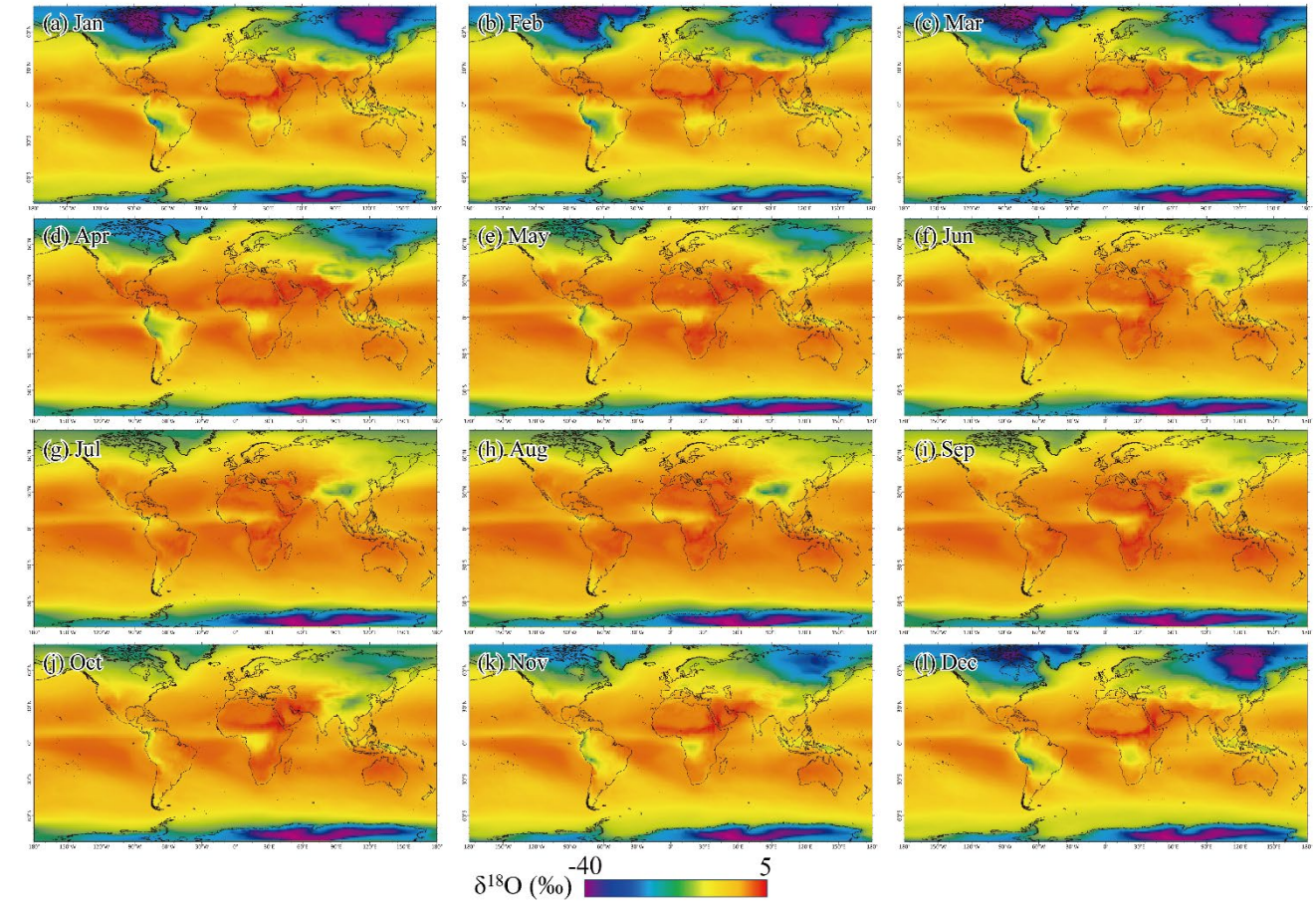

Figure 4: Climatological monthly $\delta^{18}O$ values (January–December) on a 1.25° grid averaged over 1948–2023.

https://doi.org/10.5194/essd-2026-52
Preprint. Discussion started: 20 March 2026

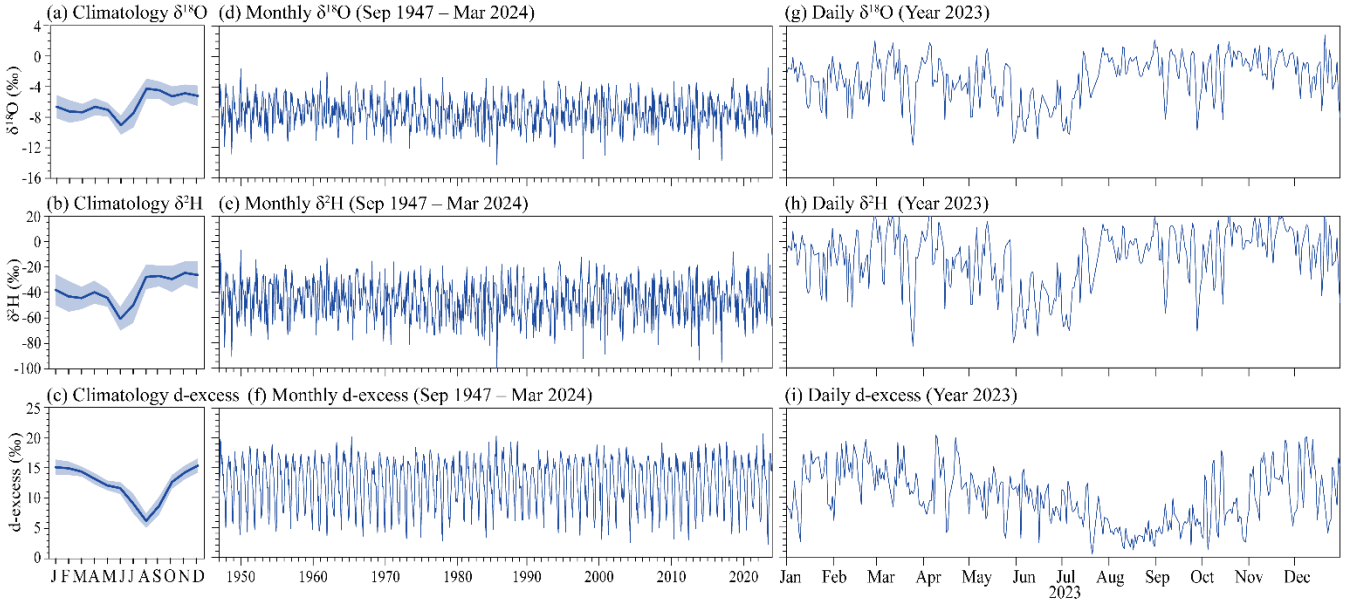

Figure 5: Precipitation-isotope time series at a representative grid cell (35°N, 140°E). Rows show $\delta^{18}O$ (a, d, and g), $\delta^{2}H$ (b, e, and h), and d-excess (c, f, and i). Panels (a–c) show the climatological monthly cycles (mean over 1948–2023; shading denotes ±1 standard deviation across years). Panels (d–f) show the precipitation-weighted monthly series (Sep 1947–Mar 2024). Panels (g–i) show the daily series for 2023.

https://doi.org/10.5194/essd-2026-52
Preprint. Discussion started: 20 March 2026

Open Access Earth System Science Data Discussions

4 Technical validations

4.1 Climatological monthly means

We summarize the validation of climatological monthly means. Pooling all the station–month pairs, the overall R^2 is 0.86 for $\delta^{18}O$ (0.87 for δ^2H), with an RMSE of 2.02‰ (16.0‰) (Fig. 6). R^2 is generally higher over continents and lower at oceanic sites. In contrast, RMSE exhibits the opposite pattern, with smaller values over the ocean and locally larger values over land (Fig. 7). These patterns indicate that the model broadly captures isotope values, whereas the seasonal phase and amplitude depend on the regional hydroclimate.

Over North America and Europe, many stations exceed $R^2 > 0.8$, indicating that the seasonal cycle is well reproduced. The typical sites (Ottawa, Bad Salzuflen, Vienna, Calgary) where phase agreement persists throughout the year are illustrated in Figure 8a–d. In these regions, the annual correction primarily trims amplitude bias and lowers the RMSE. This suggests that the timing of high and low δ values is already well captured. Along the western margin of North America, however, some locations retain errors > 5‰ for $\delta^{18}O$ (> 40‰ for δ^2H) even after correction. At Calgary, the uncorrected model exhibits a substantial positive bias. The correction markedly improves the fit, yet residual errors remain. Residual errors likely reflect sparse station density that limits jackknife interpolation across steep orographic gradients west of Calgary.

At lower latitudes (Fig. 8e–h) and in the Southern Hemisphere (Fig. 8i–l), the performance varies across sites but is broadly consistent with regional seasonality. In Bangkok (Fig. 8h), where the monsoon imposes sharp wet–dry transitions (Wang and LinHo, 2002), the model attains $R^2 = 0.97$, with an RMSE = 0.59‰. The phase is accurate, and the amplitude is well captured after correction. In Entebbe (Fig. 8f), which is representative of East Africa's bimodal rainfall regime (Nicholson, 2017), there is a corresponding bimodality in the δ cycle, with two seasonal minima. The model slightly overestimates the amplitude but preserves the phase ($R^2 = 0.74$, RMSE = 1.12‰).

Across many oceanic sites, R^2 is relatively low (often <0.5), whereas the RMSE remains small, typically < 2‰ for $\delta^{18}O$ (< 16‰ for δ^2H). The weak correlation reflects the less pronounced and more variable seasonal structure over the open ocean. In Colombo, for example, the model does not reproduce the observed high δ values from May to August ($R^2 = 0.28$, RMSE = 1.86‰).

In contrast to the δ values, the skill for d-excess are lower overall (global $R^2 = 0.25$, RMSE = 4.06‰). Some coastal continental sites perform better ($R^2 > 0.6$; RMSE < 3‰), but both phase and amplitude remain less robust than for $\delta^{18}O$ and δ^2H. This behavior indicates that the difficulty previously reported for reproducing daily d-excess in the ICM (Adachi and Yamanaka, 2025a) also extends to climatological scales. Potential contributors include the single-layer model structure, uncertainties in the meteorological forcing, and heightened sensitivity of d-excess to local boundary-layer conditions. Even with an annual-mean bias correction, the sparse spatial distribution of GNIP stations may leave residual, spatially heterogeneous biases. Accordingly, d-excess should be interpreted with more caution than are $\delta^{18}O$ and δ^2H.

Relative to an observation-based annual-mean isoscape (Bowen et al., 2005), the annual-mean bias of the bias-corrected ICM is comparable to or smaller than that of the nudged isotope-enabled GCMs (Fig. S1). When climatological monthly means

https://doi.org/10.5194/essd-2026-52
Preprint. Discussion started: 20 March 2026

Open Access Earth System Science Data Discussions

were used, the correlations with the observation-based isoscape were likewise as high or higher (Fig. S2). These results indicate that the corrected ICM provides a useful and robust dynamical isoscape option for research and applications.

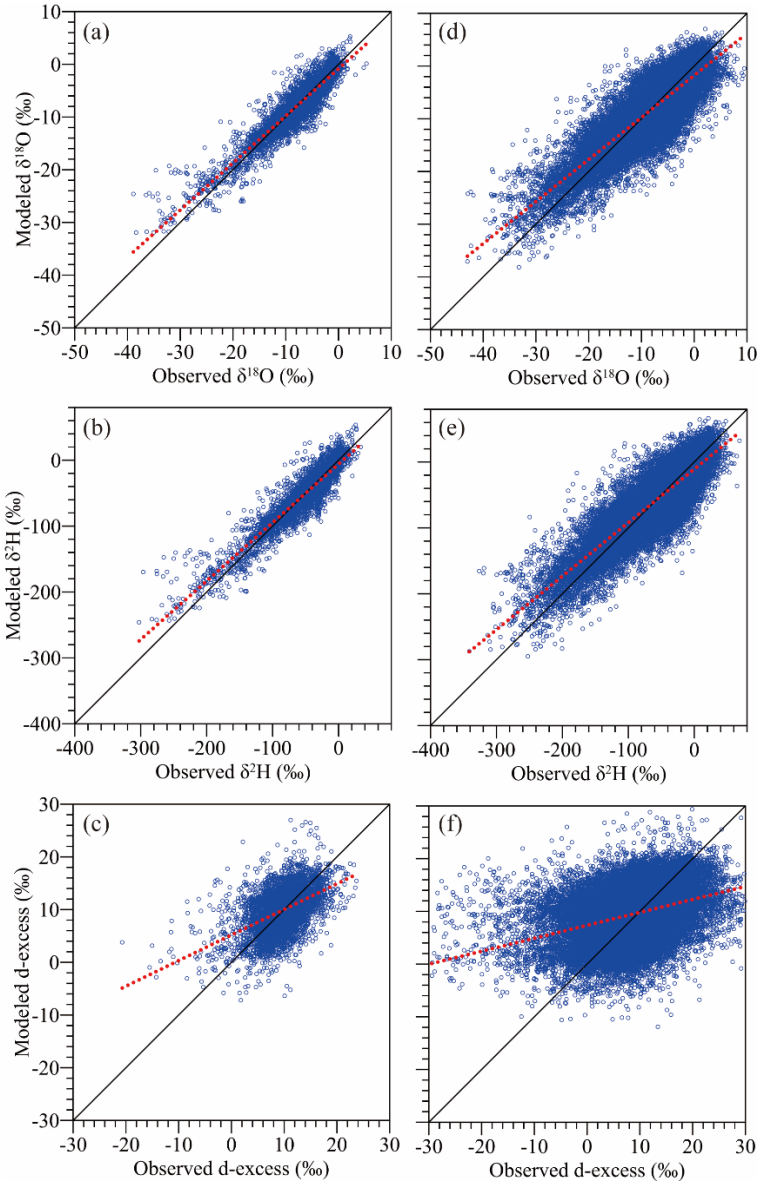

Figure 6: Stationwise model–observation comparisons for climatological means (a–c) and monthly values (d–f) from GNIP. Rows correspond to $\delta^{18}O$ (a and d), $\delta^{2}H$ (b and e), and d-excess (c and f). The blue points are station climatology (1948–2023) or station–month pairs (Sep 1947–Mar 2024). The axes show the observed values (x) versus the modeled values at the collocated grid cells (y). The black line is the 1:1 line; the red dotted line is the least-squares fit. Bias-corrected values are evaluated with leave-one-out jackknifing at station locations.

https://doi.org/10.5194/essd-2026-52
Preprint. Discussion started: 20 March 2026

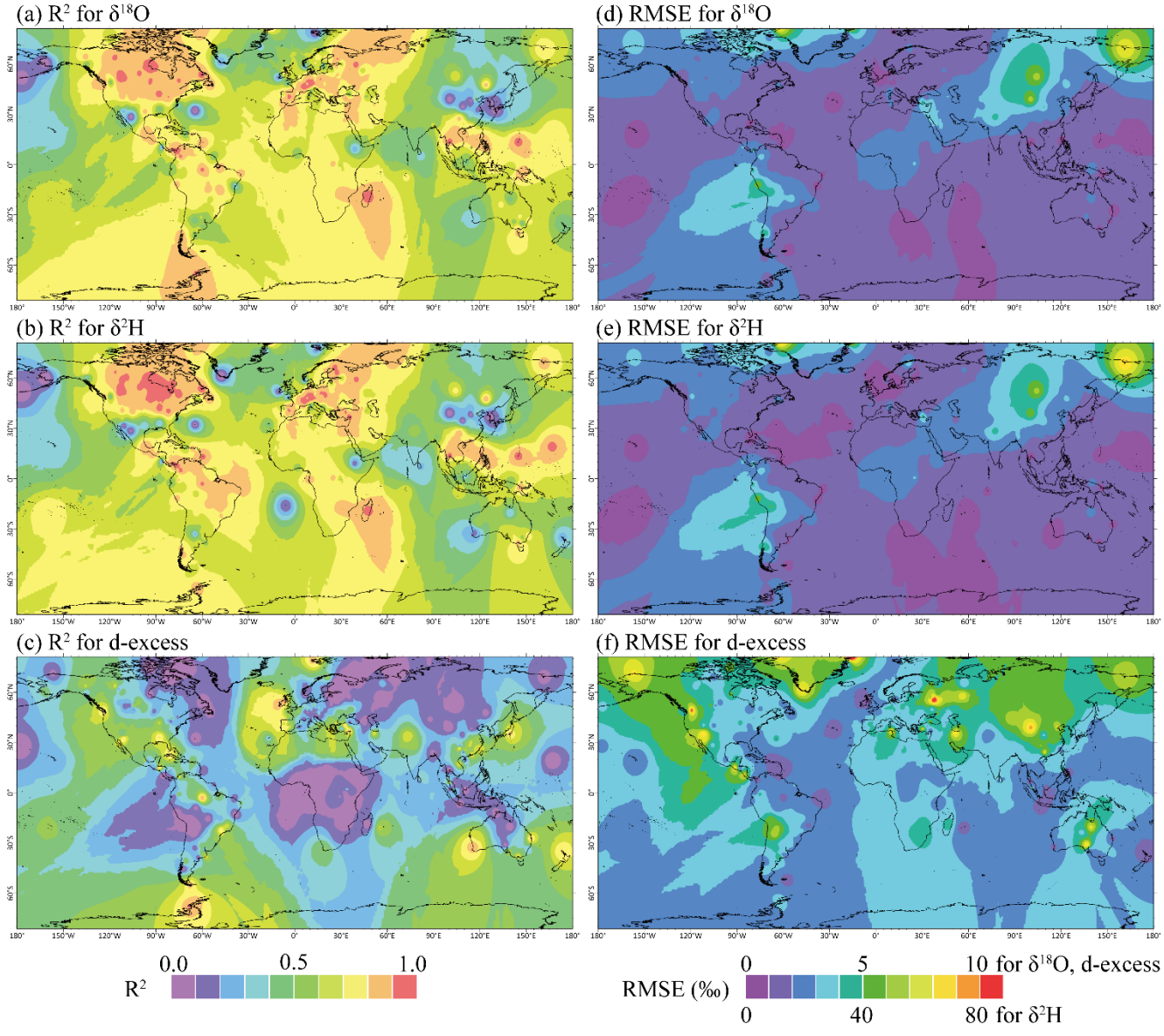

Figure 7: Global skill for climatological means (1948–2023). Columns show R^2 (a–c) and RMSE (d–f); rows correspond to $\delta^{18}O$ (a and d), δ^2H (b and e), and d-excess (c and f). Skill is computed at GNIP stations by comparing observed and modeled climatological monthly cycles at collocated grid cells and is spatially interpolated for display. Evaluations use annually bias-corrected fields with leave-one-out jackknifing.

https://doi.org/10.5194/essd-2026-52
Preprint. Discussion started: 20 March 2026

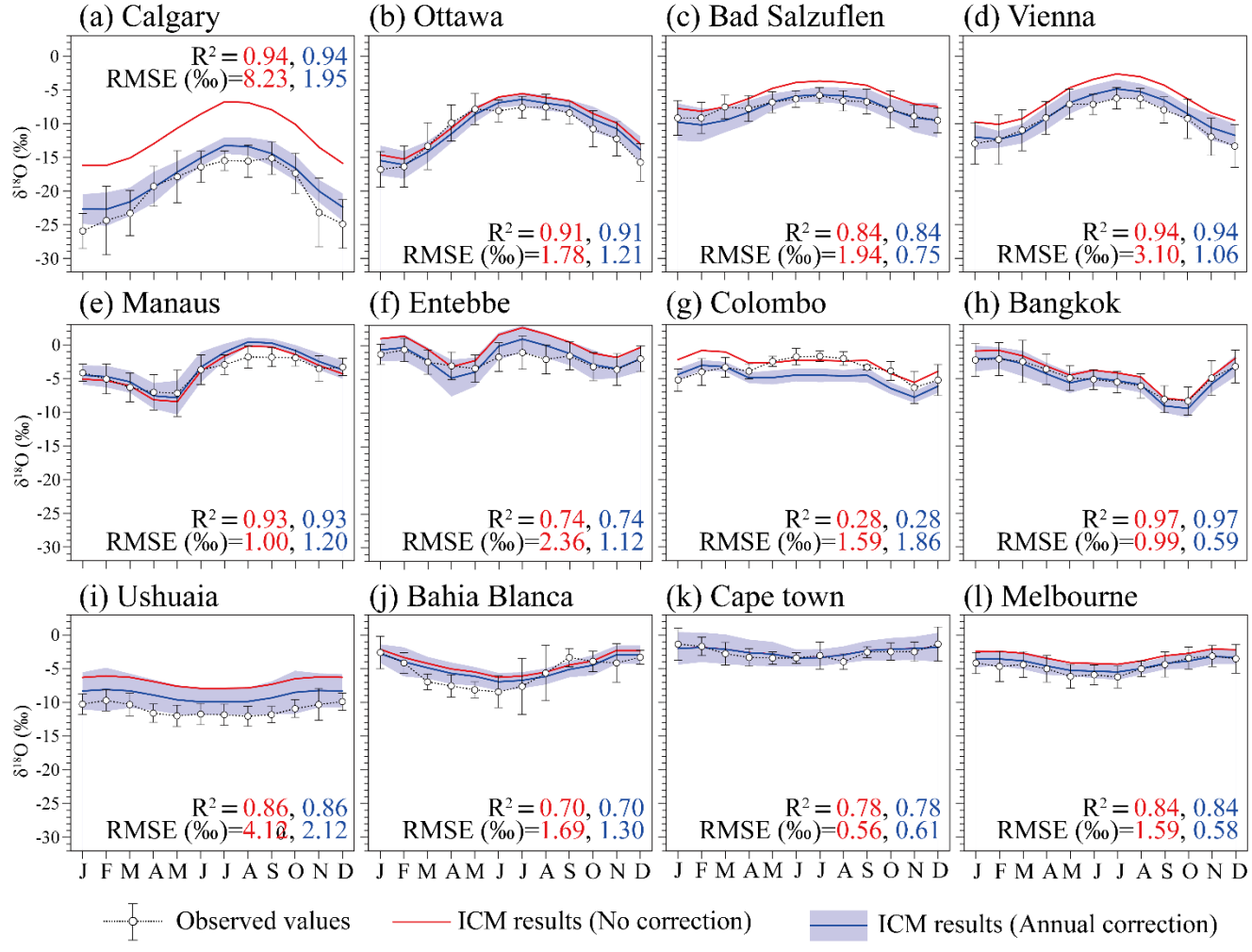

Figure 8: Climatological monthly cycles of $\delta^{18}O$ at representative GNIP stations. Circles show observed climatology; shading denotes ±1 standard deviation across years. Red lines are model results without correction; blue shading/line shows results with the annual-mean bias correction. The numbers in each panel report R^2 and RMSE (‰): red for the uncorrected model and blue for the bias-corrected model.

https://doi.org/10.5194/essd-2026-52
Preprint. Discussion started: 20 March 2026


Open Access Earth System Science Data Discussions

4.2 Monthly values

The monthly values show regional patterns similar to those of the climatology but with slightly lower skill (Fig. 9). Averaged across the stations, R^2 is 0.47 for $\delta^{18}O$ (0.48 for $\delta^{2}H$), with an RMSE of 2.62‰ (19.9‰) (Fig. 6d–e). Like the climatological results, coefficient of determinations are generally higher at continental sites (often $R^2 > 0.5$) and lower over the ocean, where seasonality is weak and synoptic-scale noise is greater.

Across mid- to high-latitude North America and Europe, several stations retain relatively high skill. Ottawa and Vienna reach $R^2 > 0.7$ for $\delta^{18}O$ with an RMSE < 2.3‰ (Fig. 10b, d), and Calgary and Bad Salzuflen exceed $R^2 > 0.5$ (Fig. 10a, c). The annual mean bias correction mainly reduces the amplitude bias and decreases the RMSE while leaving the phase coherence unchanged, which is consistent with the climatology. For example, the $\delta^{18}O$ RMSE decreases from 8.98 to 3.81‰ at Calgary, from 2.38 to 1.66‰ at Bad Salzuflen, and from 3.72 to 2.12‰ at Vienna (Fig. 9a–d).

At low latitudes, Manaus and Bangkok also have $R^2 > 0.5$, with a $\delta^{18}O$ RMSE of approximately 2‰ (Fig. 9e, h), indicating that the model captures both phase and amplitude reasonably well under strong seasonal forcing. In contrast, skill declines in the southern high latitudes and parts of eastern Eurasia, where R^2 for $\delta^{18}O$ decrease to 0.2–0.6 and the RMSE is 1.39–3.81‰ (Fig. 9i–l).

A similar geography of skill appears in the nudged isotope GCMs from SWING2 (Fig. S3). The site-level performance varies by model, but among the GCMs, the isoGSM generally performs well, and the ICM achieves comparable skill across the mid- to high-latitude Northern Hemisphere. Like ICM, GCMs tend to show reduced skill in the tropics and in the mid- to high-latitude Southern Hemisphere. For the representative GNIP stations highlighted here, ICM outperforms isoGSM at several sites, underscoring the competitiveness of the reanalysis-driven framework at monthly resolution.

Overall, the monthly skill is lower than the climatological mean skill because the month-to-month variability and sampling noise are greater. Even so, the annual correction systematically reduces the RMSE while preserving the phase, and ICM performs on par with or better than the leading isotope GCMs in many mid-latitude regions.

https://doi.org/10.5194/essd-2026-52
Preprint. Discussion started: 20 March 2026

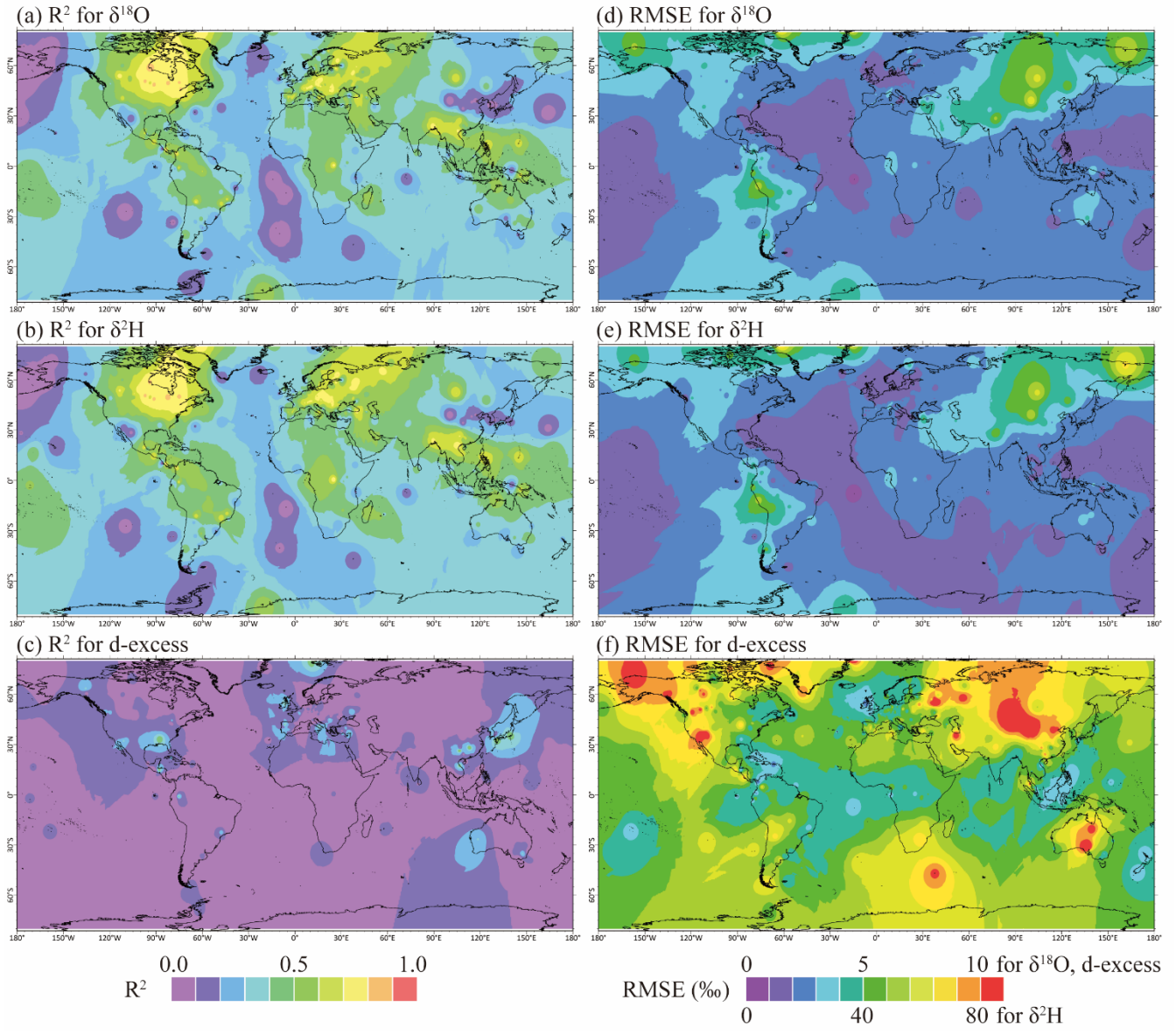

Figure 9: Global skill for monthly values (1948–2023). Columns show R^2 (a–c) and RMSE (d–f); rows correspond to $\delta^{18}O$ (a and d), δ^2H (b and e), and d-excess (c and f). Skill is computed at GNIP stations by comparing observed monthly values with the modeled precipitation-weighted monthly values at the collocated grid cells and is spatially interpolated for display. Evaluations use annually bias-corrected fields with leave-one-out jackknifing.

https://doi.org/10.5194/essd-2026-52
Preprint. Discussion started: 20 March 2026

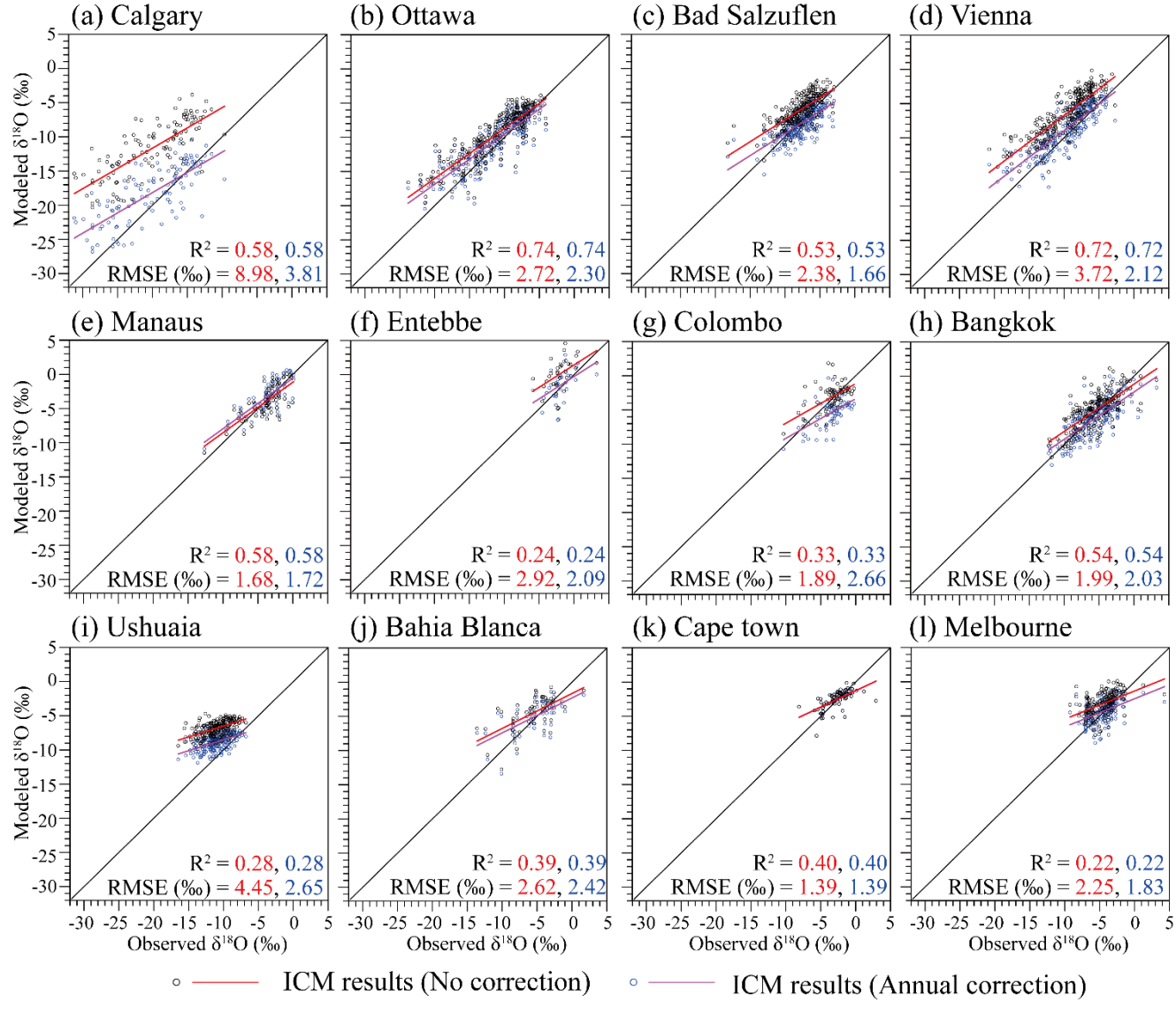

235 **Figure 10:** Monthly skill at representative GNIP stations ($\delta^{18}O$). Points are all available station–month pairs within Sep 1947–Mar 2024 (x: observed; y: modeled precipitation-weighted monthly values at the collocated grid, sampled to those months). The black line is 1:1. Red lines show least-squares fits for the uncorrected model; blue lines for the annually bias-corrected model. The numbers report R^2 and RMSE (‰): red = uncorrected, blue = bias corrected.

https://doi.org/10.5194/essd-2026-52
Preprint. Discussion started: 20 March 2026

240 **4.3 Daily values**

Under the East Asian daily evaluation, model skill is generally higher over the maritime Kanto Plain and somewhat lower over the North China Plain and the Mongolian Plateau. Without the annual-mean correction, the withheld-station evaluation yields $R^2 = 0.66$ (RMSE = 1.65‰) for the Kanto Plain, $R^2 = 0.52$ (RMSE = 3.46‰) for the North China Plain, and $R^2 = 0.49$ (RMSE = 2.98‰) for the Mongolian Plateau (Adachi and Yamanaka, 2025a). Applying the annual-mean correction and repeating the
245 evaluation leads to a substantial improvement in the North China Plain (RMSE = 2.08‰), whereas the Kanto Plain (2.08‰) and the Mongolian Plateau (3.37‰) show slight increases in the RMSE (Fig. 11). This pattern suggests that daily errors are influenced by uncertainties in meteorological controls that are not readily addressed by a constant annual offset. Despite this, the correction improves mean-level consistency and provides a practical baseline for daily analyses; further gains are expected when combined with local observations and higher-resolution meteorological fields.

250 At GNIP stations with daily observations that were not used in the correction (n = 21), $\delta^{18}O$ values typically reach R^2 values between 0.3 and 0.6, with RMSEs between 2 and 4‰, indicating that the day-to-day phase is broadly captured at many sites (Fig. 12). In contrast, d-excess is less effective in many regions, which is consistent with its greater sensitivity to forcing uncertainties and model simplifications, including the single-layer formulation.

https://doi.org/10.5194/essd-2026-52
Preprint. Discussion started: 20 March 2026

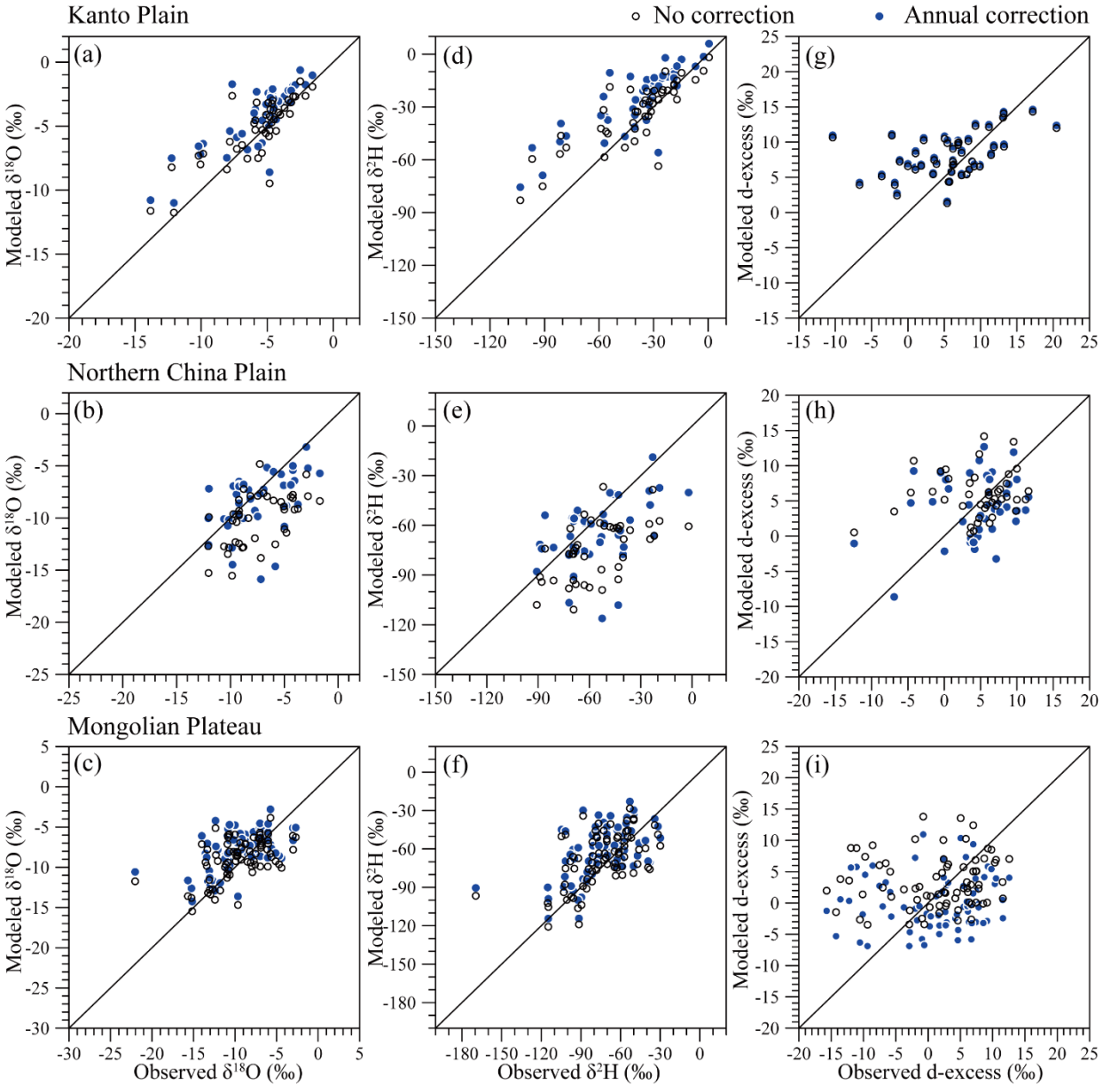

Figure 11: Regional daily skill for East Asia. Panels show the Kanto Plain (a, d, and g), North China Plain (b, e, and h), and Mongolian Plateau (c, f, and i). The columns correspond to $\delta^{18}O$ (a–c), $\delta^{2}H$ (d–f), and d-excess (g–i). The open symbols indicate no correction; the filled blue symbols indicate the annual bias-corrected model values.

https://doi.org/10.5194/essd-2026-52
Preprint. Discussion started: 20 March 2026

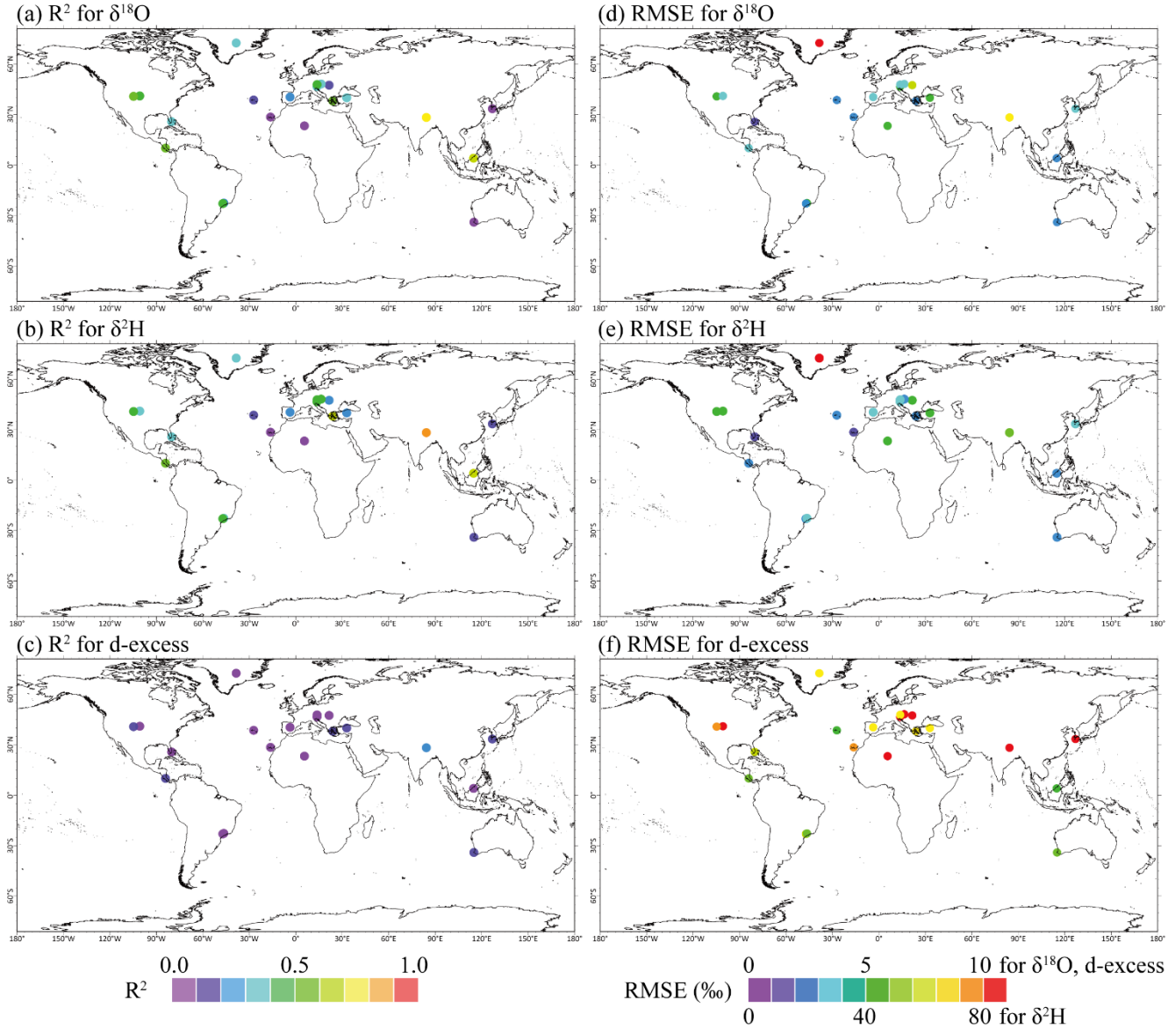

Figure 12: Daily skill at representative GNIP stations. Columns show R^2 (a–c) and RMSE (d–f); rows correspond to $\delta^{18}O$ (a and d), δ^2H (b and e), and d-excess (c and f). Metrics are computed from all available daily observations, and the observed values are compared with the modeled daily values at the collocated grid cells. Evaluations use annually bias-corrected values with leave-one-out jackknifing.

https://doi.org/10.5194/essd-2026-52
Preprint. Discussion started: 20 March 2026

5 Data availability

The dataset is archived on Zenodo under the CC BY 4.0 license. The GeoTIFF (climatology) and gridded NetCDF files (daily and monthly) are available at https://doi.org/10.5281/zenodo.18309766 (Adachi and Yamanaka, 2025b). The monthly CSV per-grid-cell time series are available at https://doi.org/10.5281/zenodo.17301045 (Adachi and Yamanaka, 2025c), and the daily CSV per-grid-cell time series at https://doi.org/10.5281/zenodo.17337279 (Adachi and Yamanaka, 2025d). Please cite this article when using the data.

6 Code availability

The IDL source code of the isotope circulation model (ICM) used in this study is archived at https://doi.org/10.5281/zenodo.18309766 (Adachi and Yamanaka, 2025b).

7 Conclusions

In this study, a global dataset of precipitation isotopic compositions computed with the isotope circulation model (ICM) and corrected for systematic biases is provided. The archive includes daily values, precipitation-weighted monthly values, and climatological monthly means on a 1.25° grid from 80° S to 80° N for September 1947–March 2024. Climatology is reproduced well, especially across continental regions, and the annual-mean bias correction further reduces the RMSE. The monthly skill is weaker than the climatological skill, but it remains of practical use. Although daily evaluations are limited in space, the simulations generally capture the observed day-to-day variability at the sites examined. In contrast, skill for d-excess is modest and warrants cautious interpretation. Accordingly, we recommend precipitation-weighted comparisons and spatial/temporal aggregation for event-scale applications. The dataset and the IDL code used to generate it are openly available. By releasing a dynamically simulated, globally evaluated isoscape, we provide a reusable foundation for tracer applications in hydrology and climate research.

Author contributions

TY conceptualized the study and supervised the research. IA carried out the simulations, data processing, and validation. IA drafted the manuscript; both authors discussed the results and edited the paper.

Competing interests

The authors declare that they have no competing interests.

https://doi.org/10.5194/essd-2026-52
Preprint. Discussion started: 20 March 2026

Open Access Earth System Science Data Discussions

Acknowledgments

We acknowledge the isotope circulation model (ICM) developed by Yoshimura et al. (2003), which formed the basis of the simulations in this study. We also acknowledge the use of the JRA-3Q reanalysis datasets. GNIP data were obtained from the IAEA WISER portal; we thank the IAEA/WMO and all GNIP contributors for maintaining and sharing these records.

Financial support

This work was supported by JSPS KAKENHI (Grant Numbers JP19H01370, JP24K00169, and JP24KJ0493).

References

Adachi, I. and Yamanaka, T.: Isotopic evolutionary track of water due to interaction with rocks and its use for tracing water cycle through the lithosphere, *J. Hydrol.*, **628**, 130589, https://doi.org/10.1016/j.jhydrol.2023.130589, 2024.

Adachi, I. and Yamanaka, T.: Evaporative effects on day-to-day precipitation isotope variability in East Asia, *Prog. Earth Planet. Sci.*, **12**, 71, https://doi.org/10.1186/s40645-025-00744-0, 2025a.

Adachi, I. and Yamanaka, T.: Global climatology, monthly, daily precipitation isotope dataset, 1947–2024 [data set], https://doi.org/10.5281/zenodo.18309766, 2025b.

Adachi, I. and Yamanaka, T.: Global monthly precipitation isotope dataset, 1947–2024 [data set], https://doi.org/10.5281/zenodo.17301045, 2025c.

Adachi, I. and Yamanaka, T.: Global daily precipitation isotope dataset, 1947–2024 [data set], https://doi.org/10.5281/zenodo.17337279, 2025d.

Birkel, C., Soulsby, C., Tetzlaff, D., Dunn, S., and Spezia, L.: High-frequency storm event isotope sampling reveals time-variant transit time distributions and influence of diurnal cycles, *Hydrol. Process.*, **26**, 308–316, https://doi.org/10.1002/hyp.8210, 2012.

Bowen, G. J. and Wilkinson, B.: Spatial distribution of $\delta^{18}O$ in meteoric precipitation, *Geology*, **30**, 315–318, https://doi.org/10.1130/0091-7613(2002)030<0315:SDOOIM>2.0.CO;2, 2002.

Bowen, G. J., Wassenaar, L. I., and Hobson, K. A.: Global application of stable hydrogen and oxygen isotopes to wildlife forensics, *Oecologia*, **143**, 337–348, https://doi.org/10.1007/s00442-004-1813-y, 2005.

Bowen, G. J.: Isoscapes: spatial pattern in isotopic biogeochemistry, *Annu. Rev. Earth Planet. Sci.*, **38**, 161–187, https://doi.org/10.1146/annurev-earth-040809-152429, 2010.

Craig, H. and Gordon, L. I.: Deuterium and oxygen-18 variations in the ocean and the marine atmosphere, in: *Stable Isotopes in Oceanographic Studies and Paleotemperatures*, edited by: Tongiorgi, E., Consiglio Nazionale delle Ricerche, Laboratorio di Geologia Nucleare, Pisa, 9–130, 1965.

https://doi.org/10.5194/essd-2026-52
Preprint. Discussion started: 20 March 2026

Ehleringer, J. R., Thompson, A. H., Podlesak, D. W., Bowen, G. J., Chesson, L. A., Cerling, T. E., Park, T., Dostie, P., and Schwarcz, H.: A framework for the incorporation of isotopes and isoscapes in geospatial forensic investigations, in: *Isoscapes: Understanding Movement, Pattern, and Process on Earth Through Isotope Mapping*, edited by: West, J. B., Bowen, G. J., Dawson, T. E., and Tu, K. P., Springer, Dordrecht, 358–387, https://doi.org/10.1007/978-90-481-3354-3_17, 2010.

Gonfiantini, R.: Environmental isotopes in lake studies, in: *Handbook of Environmental Isotope Geochemistry, Vol. 2: The Terrestrial Environment B*, Elsevier, 113–163, 1986.

Hobson, K. A., Barnett-Johnson, R., and Cerling, T. E.: Using isoscapes to track animal migration, in: *Isoscapes: Understanding Movement, Pattern, and Process on Earth Through Isotope Mapping*, edited by: West, J. B., Bowen, G. J., Dawson, T. E., and Tu, K. P., Springer, Dordrecht, 273–298, https://doi.org/10.1007/978-90-481-3354-3_13, 2010.

Joussaume, S., Sadourny, R., and Jouzel, J.: A general circulation model of water isotope cycles in the atmosphere, *Nature*, **311**, 24–29, https://doi.org/10.1038/311024a0, 1984.

Kendall, C. and Caldwell, E. A.: Fundamentals of isotope geochemistry, in: *Isotope Tracers in Catchment Hydrology*, Elsevier, 51–86, https://doi.org/10.1016/B978-0-444-81546-0.50009-4, 1998.

Kosaka, Y., Kobayashi, S., Harada, Y., Kobayashi, C., Naoe, H., Yoshimoto, K., Harada, M., Goto, N., Chiba, J., Miyaoka, K., Sekiguchi, R., Deushi, M., Kamahori, H., Nakaegawa, T., Tanaka, T. Y., Tokuhiro, T., Sato, Y., Matsushita, Y., and Onogi, K.: The JRA-3Q reanalysis, *J. Meteorol. Soc. Jpn.*, **102**, 49–109, https://doi.org/10.2151/jmsj.2024-004, 2024.

Majoube, M.: Fractionnement en 18O et en deutérium entre l'eau et sa vapeur, *J. Chim. Phys.*, **68**, 1423–1436, 1971.

Mao, J. and Yan, B.: Global Monthly Mean Leaf Area Index Climatology, 1981–2015, ORNL DAAC, Oak Ridge, Tennessee, USA, https://doi.org/10.3334/ORNLDAAC/1653, 2019.

Merlivat, L.: Molecular diffusivities of $H_2{}^{16}O$, $HD^{16}O$, and $H_2{}^{18}O$ in gases, *J. Chem. Phys.*, **69**, 2864–2871, https://doi.org/10.1063/1.436884, 1978.

Merlivat, L. and Jouzel, J.: Global climatic interpretation of the deuterium–oxygen-18 relationship for precipitation, *J. Geophys. Res.*, **84**, 5029–5033, https://doi.org/10.1029/JC084iC08p05029, 1979.

Nelson, D. B., Basler, D., and Kahmen, A.: Precipitation isotope time series predictions from machine learning applied in Europe, *Proc. Natl. Acad. Sci. USA*, **118**, e2024107118, https://doi.org/10.1073/pnas.2024107118, 2021.

Nicholson, S. E.: Climate and climatic variability of rainfall over eastern Africa, *Rev. Geophys.*, **55**, 590–635, https://doi.org/10.1002/2016RG000544, 2017.

Risi, C., Noone, D., Worden, J., Frankenberg, C., Stiller, G., Kiefer, M., Funke, B., Walker, K., Bernath, P., Schneider, M., Wunch, D., Sherlock, V., Deutscher, N., Griffith, D., Wennberg, P. O., Strong, K., Smale, D., Mahieu, E., Barthlott, S., Hase, F., García, O., Notholt, J., Warneke, T., Toon, G., Sayres, D., Bony, S., Lee, J., Brown, D., Uemura, R., and Sturm, C.: Process-evaluation of tropospheric humidity simulated by general circulation models using water vapor isotopologues: 1. Comparison between models and observations, *J. Geophys. Res. Atmos.*, **117**, D05303, https://doi.org/10.1029/2011JD016621, 2012.

https://doi.org/10.5194/essd-2026-52
Preprint. Discussion started: 20 March 2026

Stevenson, J. L., Birkel, C., Nell, A. J., Tetzlaff, D., and Soulsby, C.: Effects of streamflow isotope sampling strategies on the calibration of a tracer-aided rainfall–runoff model, *Hydrol. Process.*, **35**, e14223, https://doi.org/10.1002/hyp.14223, 2021.

Stewart, M. K.: Stable isotope fractionation due to evaporation and isotopic exchange of falling waterdrops: Applications to atmospheric processes and evaporation of lakes, *J. Geophys. Res.*, **80**, 1133–1146, https://doi.org/10.1029/JC080i009p01133, 1975.

Sturm, C., Zhang, Q., and Noone, D.: An introduction to stable water isotopes in climate models: benefits of forward proxy modelling for paleoclimatology, *Clim. Past*, **6**, 115–129, https://doi.org/10.5194/cp-6-115-2010, 2010.

Terzer-Wassmuth, S., Wassenaar, L. I., Welker, J. M., and Araguas-Araguas, L. J.: Improved high-resolution global and regionalized isoscapes of δ18O, δ2H, and d-excess in precipitation, *Hydrol. Process.*, **35**, e14254, https://doi.org/10.1002/hyp.14254, 2021.

Vachon, R. W., Welker, J. M., White, J. W. C., and Vaughn, B. H.: Monthly precipitation isoscapes (δ18O) of the United States: Connections with surface temperatures, moisture source conditions, and air mass trajectories, *J. Geophys. Res. Atmos.*, **115**, D21126, https://doi.org/10.1029/2010JD014105, 2010.

Wei, Z., Yoshimura, K., Wang, L., Miralles, D. G., Jasechko, S., and Lee, X.: Revisiting the contribution of transpiration to global terrestrial evapotranspiration, *Geophys. Res. Lett.*, **44**, 2792–2801, https://doi.org/10.1002/2016GL072235, 2017.

White, J. W. C.: Stable hydrogen isotope ratios in plants: a review of current theory and some potential applications, in: *Stable Isotopes in Ecological Research*, Springer-Verlag, 142–162, 1989.

Worden, J., Noone, D., Bowman, K., and the TES Science Team: Importance of rain evaporation and continental convection in the tropical water cycle, *Nature*, **445**, 528–532, https://doi.org/10.1038/nature05508, 2007.

Yamanaka, T., Shimada, J., and Miyaoka, K.: Time–space variation in event-based isotopic composition of precipitation, *J. Jpn. Assoc. Hydrol. Sci.*, **31**, 123–133, https://doi.org/10.4145/jahs.31.4_123, 2001.

Yamanaka, T., Shimada, J., Hamada, Y., Tanaka, T., Yang, Y., Zhang, W., and Hu, C.: Hydrogen and oxygen isotopes in precipitation in the northern part of the North China Plain: climatology and inter-storm variability, *Hydrol. Process.*, **18**, 2211–2222, https://doi.org/10.1002/hyp.5525, 2004.

Yamanaka, T., Tsujimura, M., Oyunbaatar, D., and Davaa, D.: Isotopic variation of precipitation over eastern Mongolia and its implication for the atmospheric water cycle, *J. Hydrol.*, **333**, 21–34, https://doi.org/10.1016/j.jhydrol.2006.07.022, 2007.

Yoshimura, K., Oki, T., Ohte, N., and Kanae, S.: A quantitative analysis of short-term 18O variability with a Rayleigh-type isotope circulation model, *J. Geophys. Res.*, **108**, 4647, https://doi.org/10.1029/2003JD003477, 2003.

Yoshimura, K., Kanamitsu, M., Noone, D., and Oki, T.: Historical isotope simulation using reanalysis atmospheric data, *J. Geophys. Res.*, **109**, D20109, https://doi.org/10.1029/2008JD010074, 2008.

Wang, B. and LinHo: Rainy season of the Asian–Pacific summer monsoon, *J. Climate*, **15**, 386–398, https://doi.org/10.1175/1520-0442(2002)015<0386:RSOTAP>2.0.CO;2, 2002.